Int. J. Electrochem. Sci., 7 **(2012)** 3222 - 3241

International Journal of
ELECTROCHEMICAL
SCIENCE
www.electrochemsci.org

Study of Some Bidentate Schiff Bases of Isatin as Corrosion Inhibitors for Mild Steel in Hydrochloric Acid Solution

Ashish Kumar Singh[1,*], *M. A. Quraishi*[2]

[1] Department of Chemistry, North West University (Mafikeng Campus), Mmabatho, 2735, South Africa
[2] Department of Applied Chemistry, Institute of Technology, Banaras Hindu University, Varanasi 221 005 (India)
[*]E-mail: singhapc@gmail.com

Received: 9 January 2012 / *Accepted:* 26 February 2012 / *Published:* 1 April 2012

The effect of Schiff base compounds, namely, ethylenediamine bis-isatin (EDBI), hexane 1,4-diamine bis-isatin (HDBI) and thiocarbohydrazide bis-isatin (TCBI) were investigated by gravimetric, potentiodynamic polarization, electrochemical impedance spectroscopy , atomic force microscopy and scanning electron microscopy . Although effect of molecular planarity on inhibition efficiency is observed from the results obtained between EDBI and HDBI. Adsorption of these inhibitors obeyed the Frumkin adsorption isotherm. It was found that efficiency order followed by inhibitor is TCBI>EDBI>HDBI. This fact strongly suggests that, an efficient corrosion inhibitor molecule should be large one, planar, having unoccupied d-orbital and also containing an extensive number of π-electrons.

Keywords: A-Acid solutions; A-Mild steel; B-AFM; B-EIS; C-Acid corrosion; C- Kinetic parameters

1. INTRODUCTION

Severe corrosion problems arise due to the wide use of hydrochloric acid for pickling, rescaling and cleaning processes of mild steel (MS) surfaces [1]. Due to its high mechanical properties and low cost [2], mild steel has a wide application in various industries as construction material for chemical reactors, heat exchange and boiler systems, storage tanks, and oil and gas transport pipelines. Protection of the equipments and vessels against corrosion is one of chief concerns of the maintenance and design engineers. The use of chemical inhibitors to decrease the rate of corrosion processes has been the focus of very many efforts within the chemical process industry.

Specific interaction between functional groups and the metal surface and heteroatoms like nitrogen, oxygen and sulphur play an important role in inhibition due to the free electron pairs they

posses [3-6]. Compounds that contain π-bonds generally exhibit good inhibitive properties by supplying electrons via the π-orbital. When both these features combine, enhanced inhibition can be observed.

Many studies were done on the corrosion and inhibition of steels in acidic media [7-11]. Some Schiff's bases were reported earlier as corrosion inhibitors for steel [12-15]. These substances generally become effective by adsorption on the metal surface. The adsorbed species protect the metal from the aggressive medium, which causes decomposition of the metal. Synthesized inhibitors were selected for investigation because they have -CH=N- group in the Schiff base molecules.

In this work, we studied three different Schiff base molecules which have similar chemical framework structure (Fig. 1) on the corrosion steel in 1 M HCl solution were investigated. The gravimetric and electrochemical techniques such as potentiodynamic polarization, and impedance measurements were used in this study. Steel samples were analyzed by scanning electron microscopy as well as atomic force microscopy for further confirmation. Several isotherms were tested for their relevance to describe the adsorption behaviour of the compounds studied. The effect of temperature on the corrosion behaviour of steel in the absence and presence of inhibitors was also studied.

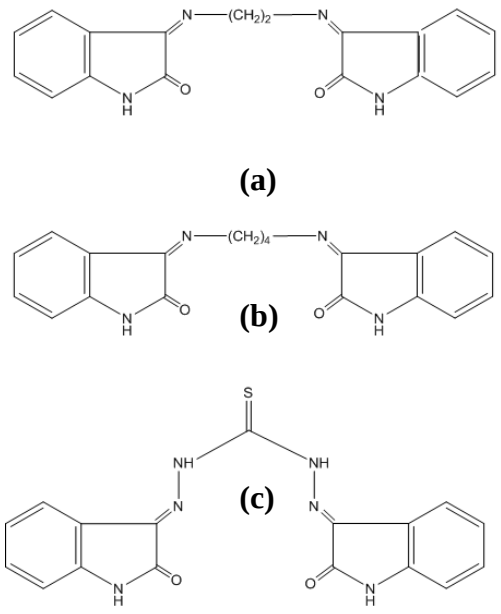

Figure 1. Structure of all the three Schiff's bases (a) EDBI, (b) HDBI and (c) TCBI

2. EXPERIMENTAL

2.1 Inhibitor

Stock solutions of all the Schiff bases were made in 10:1 ratio water: ethanol mixture by volume to ensure solubility. This stock solution was used for all experimental purposes.

2.2 Corrosion measurements

Prior to all measurements, the mild steel specimens, having composition (wt %) C = 0.17, Mn= 0.46, Si = 0.26, S = 0.017, P = 0.019 and balance Fe, were abraded successively with emery papers from 600 to 1200 mesh/in grade. The specimen were washed thoroughly with double distilled water, degreased with acetone and finally dried in hot air blower. After drying, the specimen were placed in desiccator and then used for experiment. The aggressive solution of 1 M HCl was prepared by dilution of analytical grade HCl (37%) with double distilled water and all experiments were carried out in unstirred solutions. The rectangular specimens with dimension 2.5 × 2.0 × 0.025 cm^3 were used in weight loss experiments and of size 1.0 × 1.0 cm^2 (exposed) with a 7.5 cm long stem (isolated with commercially available lacquer) were used for electrochemical measurements.

2.3 Electrochemical impedance spectroscopy

The EIS tests were performed at 308 ±1 K in a three electrode assembly. A saturated calomel electrode was used as the reference; a 1 cm^2 platinum foil was used as counter electrode. All potentials are reported versus SCE. Electrochemical impedance spectroscopy measurements (EIS) were performed using a Gamry instrument Potentiostat/Galvanostat with a Gamry framework system based on ESA 400 in a frequency range of 10^{-2} Hz to 10^5 Hz under potentiodynamic conditions, with amplitude of 10 mV peak-to-peak, using AC signal at E_{corr}. Gamry applications include software DC105 for corrosion and EIS300 for EIS measurements, and Echem Analyst version 5.50 software packages for data fitting. The experiments were carried out after 30 min. of immersion in the testing solution (no deaeration, no stirring).

The inhibition efficiency of the inhibitor was calculated from the charge transfer resistance values using the following equation:

$$\mu_{R_{ct}}\% = \frac{R_{ct}^{i} - R_{ct}^{0}}{R_{ct}^{i}} \times 100 \quad (1)$$

where, R_{ct}^{0} and R_{ct}^{i} are the charge transfer resistance in absence and in presence of inhibitor, respectively.

2.4 Potentiodynamic polarization

The electrochemical behaviour of mild steel sample in inhibited and non-inhibited solution was studied by recording anodic and cathodic potentiodynamic polarization curves. Measurements were performed in the 1 M HCl solution containing different concentrations of the tested inhibitor by changing the electrode potential automatically from -250 to +250 mV versus corrosion potential at a scan rate of 1 mV s^{-1}. The linear Tafel segments of anodic and cathodic curves were extrapolated to

corrosion potential to obtain corrosion current densities (i_{corr}). From the polarization curves obtained, the corrosion current (i_{corr}) was calculated by curve fitting using the equation:

$$I = i_{corr}\left[\exp\left(\frac{2.3\Delta E}{b_a}\right) - \exp\left(-\frac{2.3\Delta E}{b_c}\right)\right] \quad (2)$$

The inhibition efficiency was evaluated from the measured i_{corr} values using the relationship:

$$\mu_p\% = \frac{i^0_{corr} - i^i_{corr}}{i^0_{corr}} \times 100 \quad (3)$$

where, i^0_{corr} and i^i_{corr} are the corrosion current density in absence and presence of inhibitor, respectively.

2.5 Linear polarization measurement

The corrosion behaviour was studied with polarization resistance measurements (R_p) in 1 M HCl solution with and without different concentrations of studied inhibitor. The linear polarization study was carried out from cathodic potential of -20 mV versus OCP to an anodic potential of + 20 mV versus OCP at a scan rate 0.125 mV s^{-1} to study the polarization resistance ($R_{p)}$ and the polarization resistance was evaluated from the slope of curve in the vicinity of corrosion potential. From the evaluated polarization resistance value, the inhibition efficiency was calculated using the relationship:

$$\mu_{R_p}\% = \frac{R^i_p - R^0_p}{R^i_p} \times 100 \quad (4)$$

where, R^0_p and R^i_p are the polarization resistance in absence and presence of inhibitor, respectively.

2.6 Weight loss measurements

Weight loss measurements were performed on rectangular mild steel samples having size 2.5 × 2.0 × 0.025 cm^3 by immersing the mild steel coupons into acid solution (100 mL) in absence and presence of different concentrations of Schiff bases. After the elapsed time, the specimen were taken out, washed, dried and weighed accurately. All the tests were conducted in aerated 1 M HCl. All the experiments were performed in triplicate and average values were reported. From the evaluated weight loss, surface coverage (θ) was calculated using:

$$\theta = \frac{w_0 - w_i}{w_0} \quad (5)$$

where, w_0 is weight loss in free acid solution and w_i is weight loss in acid solution in presence of inhibitor, respectively.

2.7 Atomic force microscopy

The surface morphology of mild steel specimen was investigated by using atomic force microscope (AFM). Atomic force microscopy was performed using a NT-MDT multimode AFM, Russia, controlled by Solver scanning probe microscope controller. Semi-contact mode was used with the tip mounted on 100 μm long, single beam cantilever with resonant frequency in the range of 2.4×10^5-2.5×10^5 Hz, and the corresponding spring constant of 11.5 N m^{-1} with NOVA programme used for image rendering [16]. The mild steel strips of $1.0 \times 1.0 \times 0.025$ cm sizes were prepared as described in section 2.2. After immersion in 1 M HCl with and without addition of 100 ppm Schiff bases at 308 K for 3 h, the specimen were cleaned with distilled water, dried and then used for AFM.

2.8 Scanning electron microscopy

The morphology of the surface of mild steel in 1 M HCl solution in absence and presence of 100 ppm of Schiff bases was also tested by SEM examinations using a Traktor TN-2000 energy dispersive spectrometer and a Jeol-Jem-1200 EX II electron microscope in the vacuum mode by instrument operated at 10 kV.

3. RESULTS AND DISCUSSION

3.1 Electrochemical impedance spectroscopy

Impedance method provides information about the kinetics of the electrode processes and simultaneously about the surface properties of the investigated systems. The shape of impedance gives mechanistic information. Nyquist and Bode plots of mild steel in uninhibited and inhibited acid solution containing various concentrations of Schiff bases are presented in Fig. 2 and Fig. 3. It followed from Fig. 2a-c that a high frequency (HF) depressed charge-transfer semicircle was observed followed by a well defined inductive loop in the low frequency (LF) regions. The HF semicircle is attributed to the time constant of charge transfer and double-layer capacitance [17, 18]. The LF inductive loop may be attributed to the relaxation process obtained by adsorption species as Cl^-_{ads} and H^+_{ads} on the electrode surface [19].

Different corrosion parameters derived from EIS measurements are presented as Table 1. It is shown from Table 1 that R_{ct} of inhibited system increased and double layer capacitance C_{dl} decreased with increasing inhibitor concentration. This decrease in C_{dl} results from a decrease in local dielectric

constant and/or an increase in the thickness of the double layer, suggested that inhibitor molecules inhibit the iron corrosion by adsorption at the metal/acid interface [20, 21].

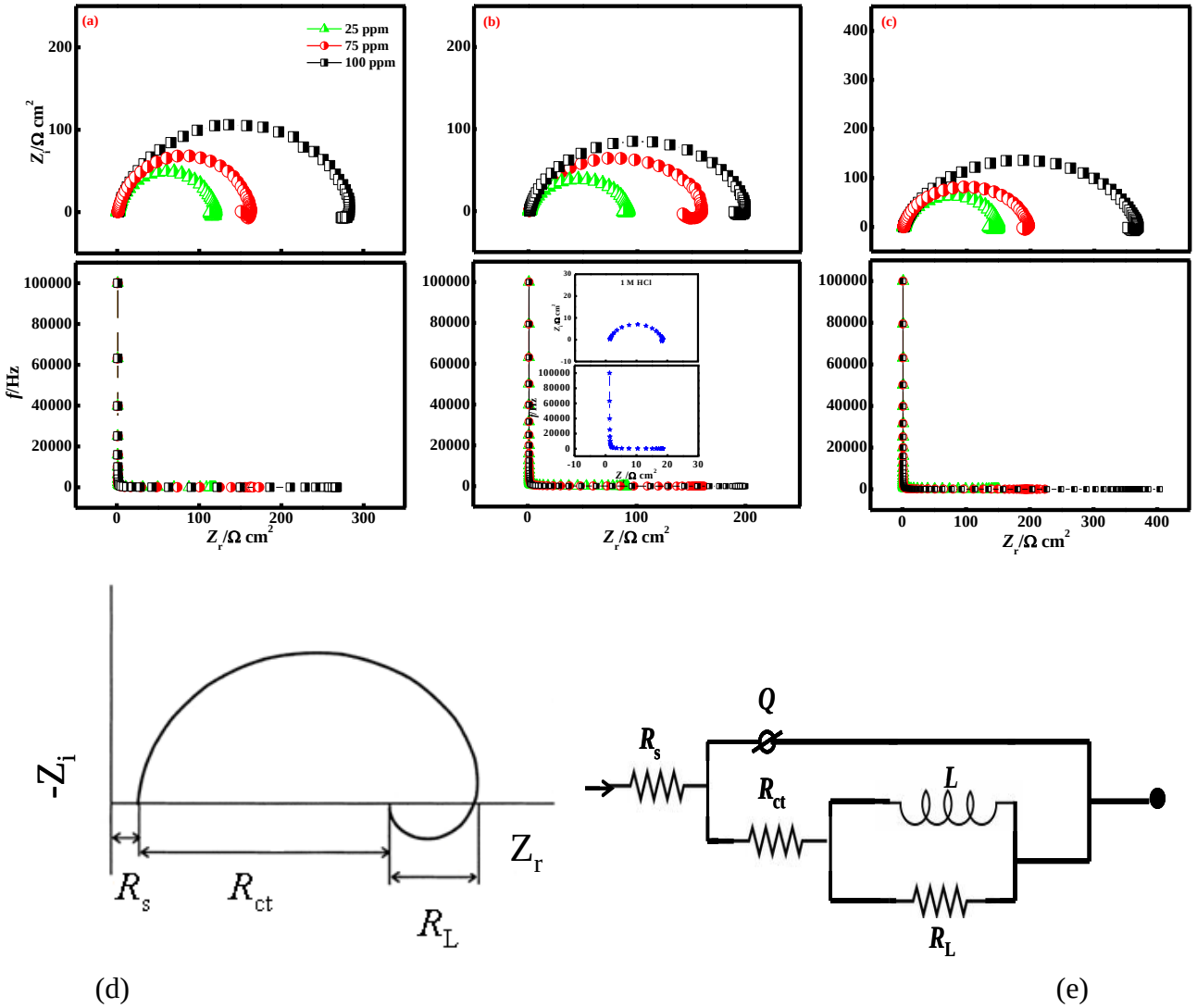

Figure 2. (a) Nyquist plots of mild steel in 1 M HCl in absence and presence of Different concentrations of EDBI, (b) HDBI, (c) TCBI, (d) illustration of simple Nyquist plot and (e) electrochemical equivalent circuit used to fit the impedance Spectra

Phase angle at high frequencies provided a general idea of anticorrosion performance. The more negative the phase angle the more capacitive the electrochemical behaviour [22]. Charge transfer resistance increment could raise current tendency to pass through the capacitor in the circuit. Also, depression of phase angle at relaxation frequency with decreasing the inhibitor concentration (Fig. 3 d-f) indicated the decrease of capacitive response with the decrease of inhibitor concentration. Such a phenomenon could be attributed to higher corrosion activity at low concentrations of inhibitor.

Fig. 2d presented a typical Nyquist diagram. To get more accurate fit of these experimental data, the measured impedance data were analysed by fitting in to equivalent circuit given in Fig. 2e. Excellent fit with this model was obtained for all experimental data. As an example, the Nyquist and bode-phase plots in uninhibited solution are presented in Figure 4 a-b. The equivalent circuit consists of the double-layer capacitance (C_{dl}) in parallel to the charge transfer resistance (R_{ct}), which is in series to the parallel of inductive elements (L) and R_L.

One constant phase element (CPE) is substituted for the capacitive element to give a more accurate fit, as the obtained capacitive loop is a depressed semi-circle.

The CPE is a special element whose admittance value is a function of the angular frequency (ω), and whose phase is independent of the frequency. The admittance and impedance of CPE is given by;

$$Y_{CPE} = Y_0(i\omega)^n \quad (6)$$

where, Y_0 is the magnitude of CPE, i is an imaginary number ($i^2 = -1$) α is the phase angle of CPE and $n = \alpha/(\pi/2)$ in which α is the phase angle of CPE.

The electrochemical parameters, Including R_s, R_{ct}, R_L, L, Y_0 and n are listed in Table 1. C_{dl} values derived from CPE parameters according to equation (7) are listed in Table 1.

$$C_{dl} = (Y_0.R_{ct}^{1-n})^{1/n} \quad (7)$$

Table 1. Calculated electrochemical parameters for mild steel in absence and presence of different concentrations of different inhibitors

Inhibitor	Conc. (ppm)	Tafel data					Linear polarization data		EIS data							
		E_{corr} (mv vs. SCE)	i_{corr} (μA cm^{-2})	β_a (mV d^{-1})	β_c (mV d^{-1})	μ_p %	R_p (Ω cm^2)	μ_{R_p} %	R_s (Ω cm^2)	Q (Ω^{-1} s^n cm^{-2})	α	L (Ω cm^2)	R_{ct} (Ω cm^2)	R_L (Ω cm^2)	C_{dl} (μF cm^{-2})	μ_{EIS} %
	-	469	730	73	127	-	18	-	1.30	164	0.811	17	16	41	41	-
EDBI	25	488	112	70	137	85	153	88	1.02	67	0.870	24	115	4	32	86
	75	490	95	68	140	87	193	91	1.05	48	0.901	57	140	19	28	89
	100	491	67	68	143	91	277	93	1.64	32	0.924	8.7	274	7	21	94
HDBI	25	491	115	68	135	84	132	86	1.03	53	0.895	3	86	5	28	82
	75	490	101	72	149	86	167	89	1.05	45	0.910	57	130	15	27	87
	100	460	72	66	150	90	191	90	1.16	32	0.929	15	188	12	21	91
TCBI	25	492	96	67	135	87	190	90	1.22	51	0.897	15	147	10	29	89
	75	471	87	71	200	88	232	92	1.08	32	0.921	100	194	5	21	92
	100	457	45	65	193	94	400	95	0.80	27	0.941	188	365	5	20	96

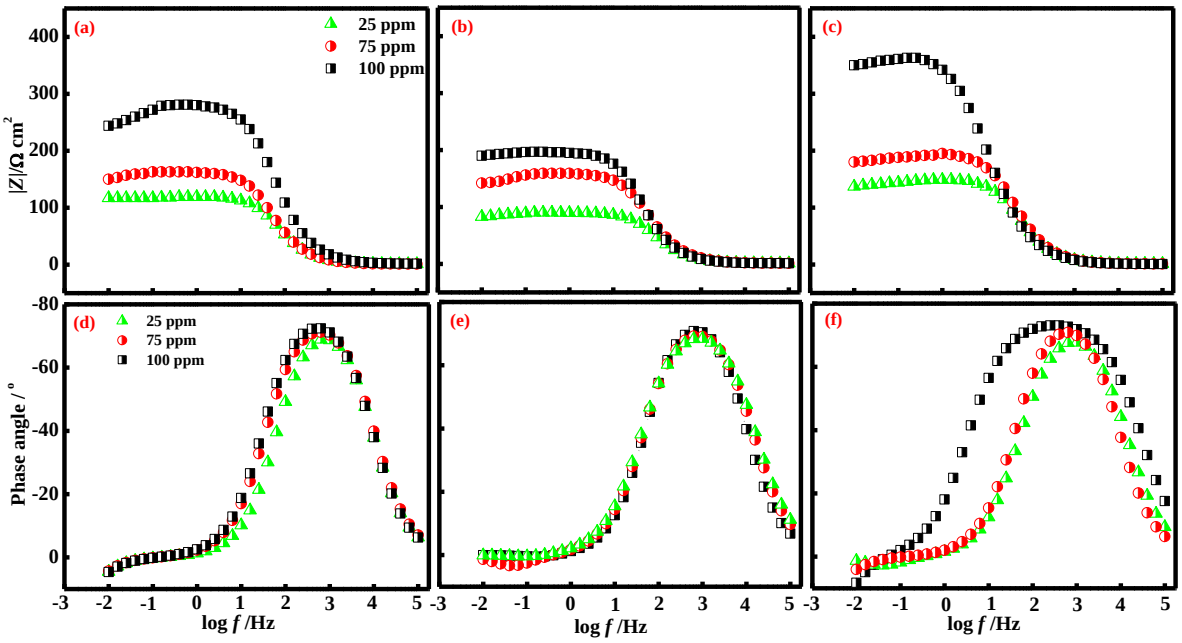

Figure 3. (a) Bode plots of mild steel in presence of different concentrations of EDBI, (b) HDBI, (c) TCBI, (d) phase angle plots of mild steel in presence of different concentrations of EDBI, (e) HDBI and (f) TCB

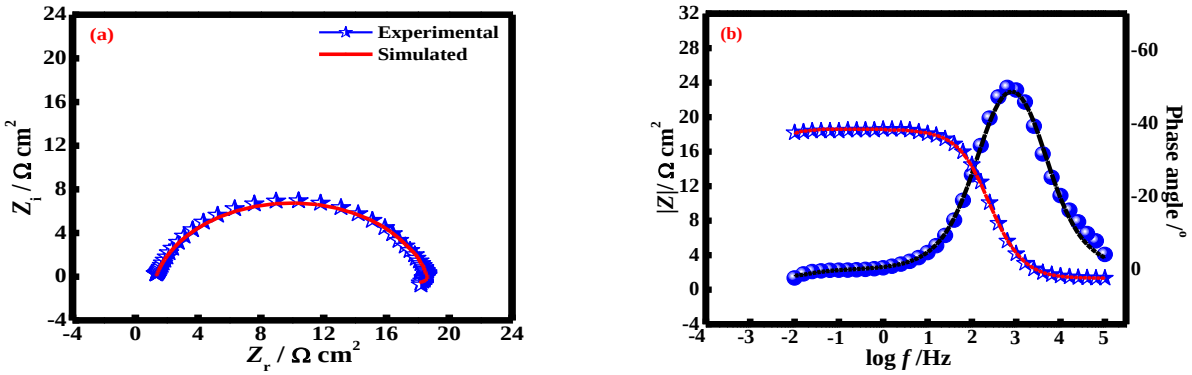

Figure 4. (a) Nyquist plot, (b) Bode-phase angle plot of iron in 1 M HCl

3.2 Potentiodynamic Polarization

The polarization curves of mild steel in hydrochloric acid solution, in the absence and presence of different concentrations of studied inhibitors, are presented in Fig. 5 and quantified in Table 1. The maximum inhibition efficiency (94%) was obtained in TCBI at a concentration of 100 ppm.

Addition of the Schiff bases to acid media affected both the cathodic and anodic parts of the curves. Therefore, these compounds behave as mixed inhibitors. From the polarization curves it was noted that the curves were shifted toward lower current density region and β_c values increased with increase of concentration of inhibitor compounds. The higher β_c values indicated the retardation of

cathodic reduction rate. Hence, the Schiff's bases influenced cathodic reaction more rather than anodic reaction and the addition of Schiff's bases controls the rate of hydrogen evolution reaction on mild steel surface. The shift in the anodic Tafel slope β_c may be due to the chloride ions/or inhibitor molecules adsorbed onto steel surface. The inhibition efficiency values in the Table 1 showed that the Schiff's bases act as very effective corrosion inhibitors for mild steel in HCl solution and their capacity of inhibition increased with increase of concentration.

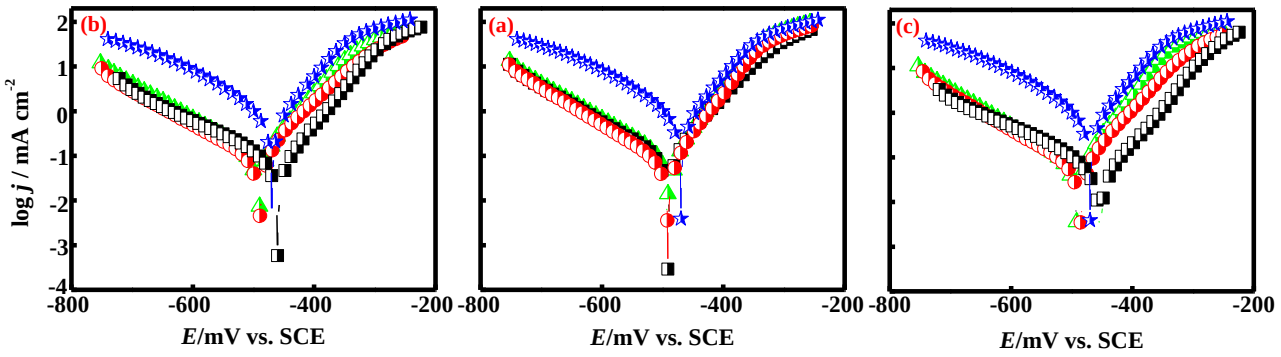

Figure 5. Typical polarization curves for corrosion of mild steel in 1 M HCl in the absence and presence of different concentrations of (a) EDBI, (b) HDBI and (c) TCBI

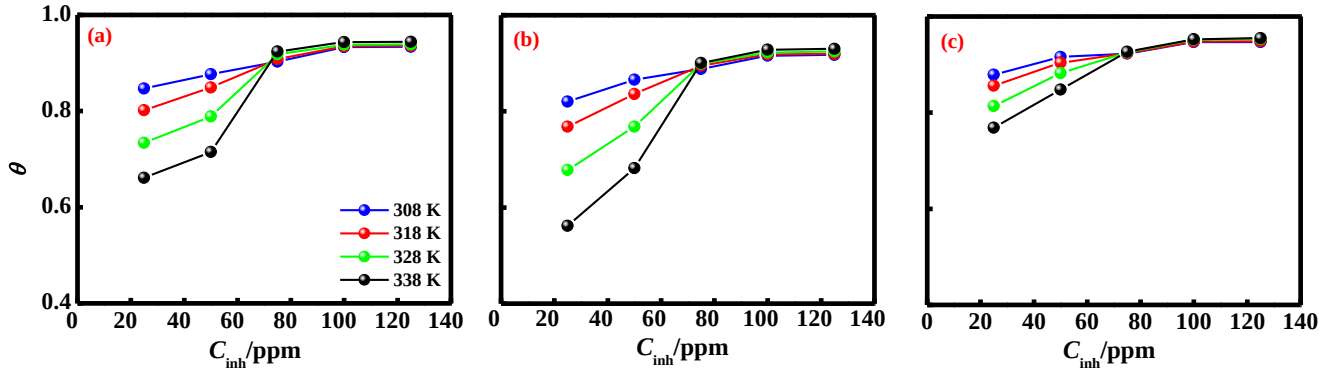

Figure 6. Variation of surface coverage with concentration of (a) EDBI, (b) HDBI and (c) TCBI

Further, the concentration of inhibitors employed for the study was very small and indicated the great deal of activeness of these compounds to steel surface.

As it can be seen from Table 1, the studied inhibitors reduced both anodic and cathodic currents with a slight shift in corrosion potential (≈ 25 mV). According to Ferreira and others [23, 24], if the displacement in corrosion potential is more than 85 mV with respect to corrosion potential of the blank solution, the inhibitor can be seen as a cathodic or anodic type. In the present study, the maximum displacement was 22 with EDBI, 22 with HDBI and 23 mV with TCBI which indicated that the studied inhibitors acted as mixed type.

3.3 Linear polarization measurement

The inhibition efficiencies and polarization resistance parameters are presented in Table 1. The results obtained from Tafel polarization and EIS showed good agreement with the results obtained from linear polarization resistance.

3.4 Weight loss measurements

3.4.1 Effect of inhibitor concentration

The effect of inhibitor concentration on inhibition efficiency of steel in 1 M HCl was first examined. Fig. 6 a-c represented such behaviour in the presence of different concentration of all the three Schiff's bases in 1 M HCl. Maximum inhibition efficiency was shown at 100 ppm in HCl solution. The values of percentage inhibition efficiency (μ_{WL}%) and corrosion rate (C_R) obtained from weight loss method at different concentrations of all the Schiff bases at 308 K are summarized in Table 2.

Table 2. Corrosion rate and Inhibition efficiency values for the corrosion of mild steel in aqueous solution of 1 M HCl in the absence and in the presence of different concentrations of different inhibitors from weight loss measurements at 308 K

Name of Inhibitor	Conc. of Inhibitor (ppm)	Surface Coverage (θ)	μ_{WL}%	C_R (mmy^{-1})
-	-	-	-	40.4
EDBI	25	0.85	85	6.2
	50	0.88	88	5.0
	75	0.90	90	3.9
	100	0.93	93	2.7
	125	0.93	93	2.7
HDBI	25	0.82	82	7.1
	50	0.86	86	5.4
	75	0.89	89	4.5
	100	0.92	91	3.4
	125	0.92	92	3.3
TCBI	25	0.88	88	4.9
	50	0.92	91	3.4
	75	0.92	92	3.1
	100	0.95	95	2.1
	125	0.95	95	2.1

3.4.1 Effect of temperature

In order to investigate the effect of temperature on the performance of studied inhibitors and to derive thermodynamic activation parameters and thermodynamic parameters of adsorption, weight loss

studies were performed at four different temperatures. The inhibition efficiency of all the three studied inhibitors remains almost constant (slightly increased) with increasing temperature.

3.4.3 Thermodynamic activation parameters

The dependence of corrosion rate at temperature can be expressed by Arrhenius equation and transition state equation:

$$\log(C_{\mathrm{R}}) = \frac{-E_{\mathrm{a}}}{2.303RT} + \log\lambda \tag{8}$$

$$C_{\mathrm{R}} = \frac{RT}{Nh}\exp\left(\frac{\Delta S^{*}}{R}\right)\exp\left(-\frac{\Delta H^{*}}{RT}\right) \tag{9}$$

where E_{a} apparent activation energy, λ the pre-exponential factor, ΔH^{*} the apparent enthalpy of activation, ΔS^{*} the apparent entropy of activation, h Planck's constant and N the Avogadro number, respectively.

The apparent activation energy and pre-exponential factors for a wide range of concentration of Schiff's bases can be calculated by method described elsewhere [25] and the results are presented as Table 3. Figure 7 depicted an Arrhenius plots for mild steel immersed in 1 M HCl in presence of different concentration of Schiff's bases. Table 3 included E_{a} values for a wide range of concentration of the three inhibitors tested. Inspection of Table 3 showed that at lower concentration of all the inhibitor, activation energy increased compared to the free acid solution. The increase in E_{a} could be interpreted as the physical adsorption which occurs in the first stage [26-29]. At highest concentration, activation energy was found to decrease for all the three Schiff's bases.

The $Fe(Inh)_{ads}$, reaction intermediates $Fe + Inh \leftrightarrow Fe(Inh)_{ads} + Fe^{n+} + ne^{-} + Inh$ can explain the inhibition mechanism. At first, when there is not enough $Fe(Inh)_{ads}$ to cover the metal surface, because the inhibitor concentration is low or because the adsorption rate is slow, metal dissolution takes place on the mild steel surface free of $Fe(Inh)_{ads}$. With high inhibitor concentration a compact and coherent inhibitor layer is formed on the mild steel which reduces chemical attack on the metal.

As it can be seen from Table 3, the values of activation free energy of all the three studied are higher than that of free acid solution at lower concentration and lower at higher concentration. Thus, the corrosion rate of mild steel is mainly controlled by activation parameters at lower concentration and by pre-exponential factor at higher concentration.

The relationship between $\log(C_{\mathrm{R}}/T)$ and $1/T$ were shown in Figure 7d-f. Straight lines are obtained with a slope $(-\Delta H^{*}/2.303R)$ and an intercept of $\left[\log(R/Nh)+(\Delta S^{*}/2.303R)\right]$, from which the value of ΔH^{*} and ΔS^{*} were calculated and presented in Table 2. The positive sign of enthalpy reflect the endothermic nature of steel dissolution process meaning that dissolution of steel is difficult. On comparing the values of entropy of activation (ΔS^{*}) listed in Table 3, it is clear that entropy of

activation decreased in presence of the higher concentration of inhibitors compared to free acid solution. The decreased entropy of activation in the presence of inhibitors indicated that disorderness is decreased on going from reactant to activated complex.

Table 3. Thermodynamic activation parameters for mild steel in 1 M HCl in absence and presence of different concentrations of different inhibitors.

Inhibitor	Conc. (ppm)	E_a (kJ mol^{-1})	λ (mg cm^{-2})	ΔH^* (kJ mol^{-1})	ΔS^* (J mol^{-1} K^{-1})	ΔG^* (kJ mol^{-1})			
						308 K	318 K	328 K	338 K
	-	42	5.3×10^{8}	40	-87	66.8	67.7	68.5	69.4
EDBI	25	66	8.8×10^{11}	63	-88	71.6	71.8	72.2	72.5
	50	68	11.8×10^{11}	64	-25	71.7	71.9	72.2	72.4
	75	35	3.6×10^{6}	32	-125	70.5	71.7	73.0	74.2
	100	38	7.3×10^{6}	35	-124	73.2	74.4	75.7	76.9
	125	38	7.1×10^{4}	35	-124	73.2	74.4	75.7	76.9
HDBI	25	69	3.6×10^{12}	66	-16	70.9	71.1	71.2	71.4
	50	68	1.7×10^{12}	64	-22	70.8	71.0	71.2	71.4
	75	39	2.0×10^{7}	36	-116	71.7	72.9	74.0	75.2
	100	38	9.9×10^{6}	35	-121	72.3	73.5	74.7	75.9
	125	38	8.0×10^{6}	35	-123	72.9	74.1	75.3	76.6
TCBI	25	62	1.3×10^{11}	59	-43	72.2	72.7	73.1	73.5
	50	60	4.6×10^{10}	57	-52	73.0	73.5	74.0	74.6
	75	40	2.7×10^{7}	38	-113	72.8	79.3	75.0	76.2
	100	39	9.7×10^{6}	36	-122	73.6	74.8	76.0	77.2
	125	38	5.4×10^{6}	35	-126	73.8	75.0	76.3	77.6

The change in activation free energy (ΔG^*) of the corrosion process can be calculated at each temperature by applying known equation:

$$\Delta G^* = \Delta H^* - T\Delta S^* \quad (10)$$

The obtained ΔG^* values were also listed in Table 3. The values of ΔG^* were positive and showed limited increase with rise in temperature, indicating that the activated complex was not stable and the probability of its formation decreased some what with rise in temperature. However,

ΔG^* values for inhibited systems revealing that in cores of inhibitor addition the activated corrosion complex becomes less stable as compared to its absence.

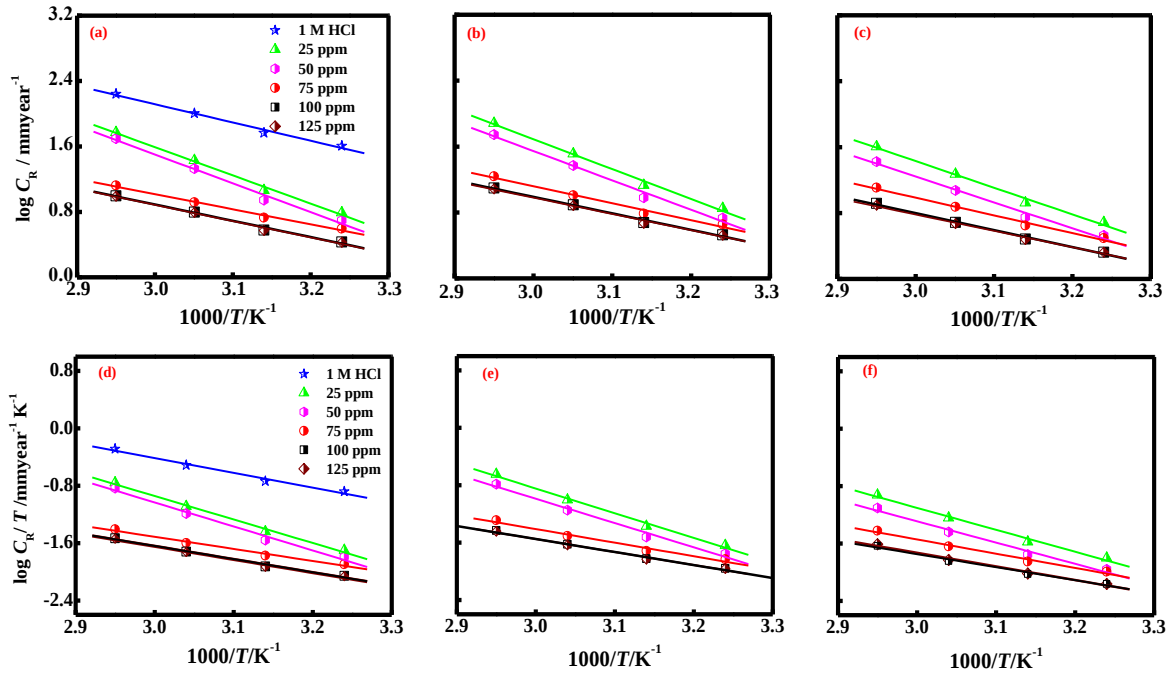

Figure 7. Adsorption isotherm plots for (a) log *C*R versus 1/*T* at different concentrations of EDBI, (b) HDBI, (c) TCBI, (d) log *C*R/*T* versus 1/*T* at different concentrations of EDBI, (e) HDBI and (f) TCBI

3.4.4 Thermodynamic parameters and adsorption isotherm

The efficiency of Schiff bases molecules as a successful corrosion

Inhibitor mainly depends on their adsorption ability on the metal surface. To emphasize the nature of adsorption, the adsorption of an organic adsorbate at metal/solution interface can be presented as a substitution adsorption process between the organic molecules in aqueous solution $Org_{(sol)}$, and the water molecules on metallic surface $H_2O_{(ads)}$:

$$Org_{(sol)} + xH_2O_{(ads)} \quad Org_{(ads)} + xH_2O_{(sol)} \qquad (11)$$

where, $Org_{(sol)}$ and $Org_{(ads)}$ are the organic molecules in the solution and adsorbed on the metal surface, respectively, and n is the number of water molecules replaced by the water molecules. It is essential to know the mode of adsorption and the adsorption isotherm that can give important information on the interaction of inhibitor and metal surface. The surface coverage value, θ ($\theta = \mu_{WL}\%/100$) for different concentrations of Schiff bases was used to explain the best adsorption isotherm. Attempts were made to fit surface coverage values determined from weight loss

measurements into different adsorption isotherm models (Figure 8). The linear regression coefficient values (R^2) determined from the plotted curves were found to be in the range of 0.9992-0.9999 for Langmuir, 0.8763-0.9854 for Temkin and 0.9179-0.9663 for Frumkin adsorption isotherms at different temperatures studied. According to these results, it can be concluded that the best description of the adsorption behaviour of all the three studied Schiff's bases can be best explained by Langmuir adsorption isotherm given by equation (12).

Langmuir adsorption isotherm can be expressed by following equation:

$$\frac{C_{(inh)}}{\theta} = \frac{1}{K_{(ads)}} + C_{(inh)} \qquad (12)$$

where, C_{inh} is inhibitor concentration and K_{ads} is an equilibrium constant for adsorption-desorption process.

The standard free energy of adsorption of inhibitor (ΔG^{o}_{ads}) on mild steel surface can be evaluated with the following equation:

$$\Delta G^{o}_{ads} = -RT \ln(55.5 K_{ads}) \qquad (13)$$

The negative values of standard free energy of adsorption indicated spontaneous adsorption of Schiff bases on mild steel surface and also strong interaction and stability of the adsorbed layer with the steel surface [30].

The calculated standard free energy of adsorption value for all the three Schiff bases is closer to -40 kJ mol^{-1}. Therefore, it can be concluded that the adsorption of Schiff bases on the mild steel surface is more chemical than physical one [31].

Table 4. Thermodynamic parameters for the adsorption of inhibitors in 1 M HCl on the mild steel at different temperatures

Inhibitor	**Conc. (ppm)**	***T* (K)**	**K_{ads} (10^4 M^{-1})**	**- ΔG^{o}_{ads} (kJ mol^{-1})**	**ΔH^{o}_{ads} (kJ mol^{-1})**	**ΔS^{o}_{ads} (J K^{-1} mol^{-1})**
EDBI	100	308	4.4	38	26	171
		318	4.6	39		
		328	4.8	40		
		338	5.3	42		
HDBI	100	308	3.8	37	24	147
		318	3.9	39		
		328	4.1	40		
		338	4.5	41		
TCBI	100	308	6.5	39	20	129
		318	6.6	40		
		328	7.2	41		
		338	7.3	43		

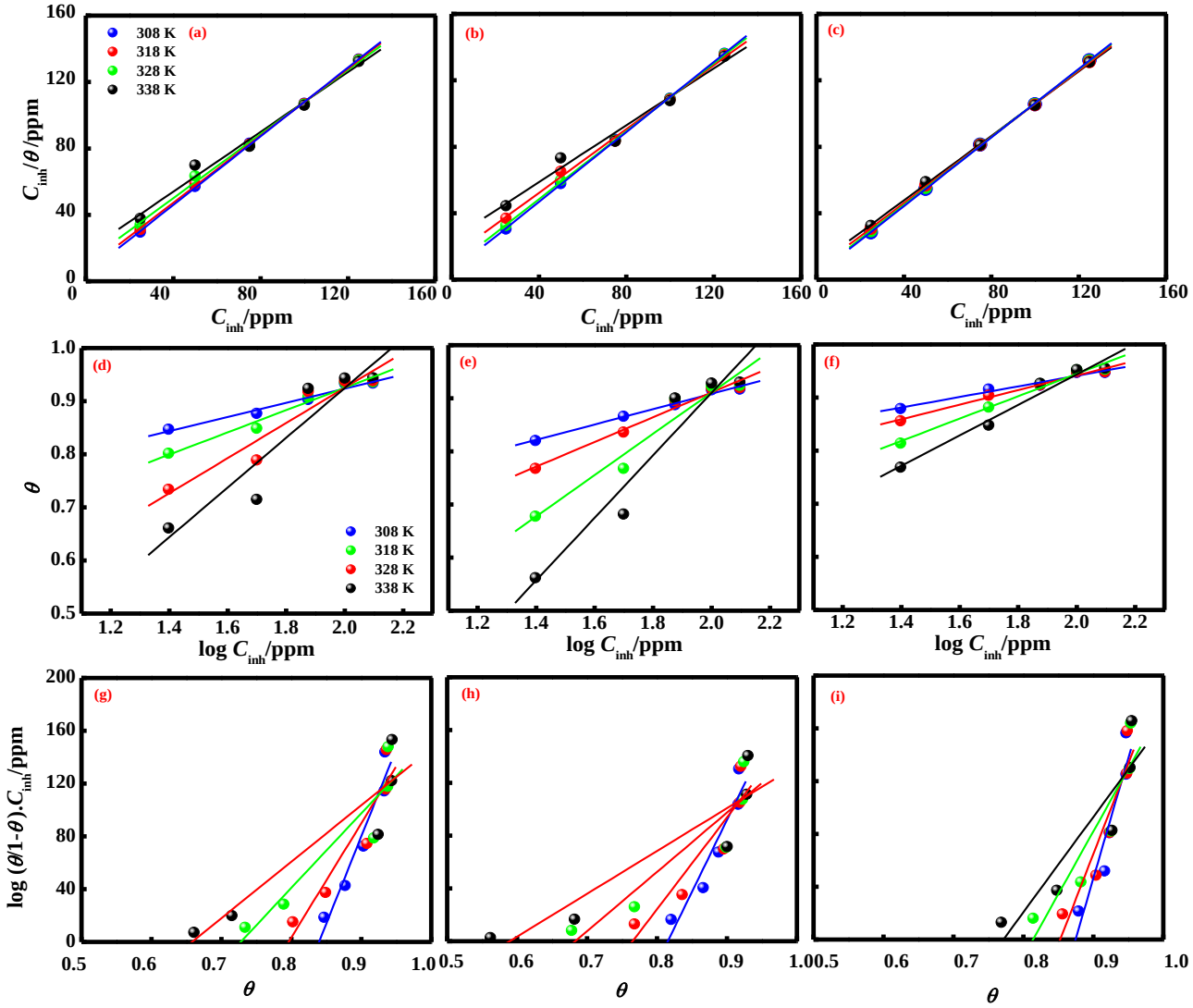

Figure 8. (a), (b), (c) Langmuir adsorption isotherm plots for the adsorption of EDBI, HDBI and TCBI in 1 M HCl on the surface of mild steel, (d), (e), (f) Temkin isotherm plots for EDBI, HDBI and TCBI, (g), (h) and (i) Frumkin isotherm plots for the adsorption of EDBI, HDBI and TCBIAccording to Van't Hoff equation [32]:

$$\ln K_{ads} = \frac{-\Delta H^{o}_{ads}}{RT} + \text{constant} \qquad (14)$$

To calculate heat of adsorption $\ln K_{ads}$ was plotted against $1/T$, as shown in Figure 9. The straight lines were obtained with slope equal to $(-\Delta H^{o}_{ads}/R)$ and intercept equal to $(\Delta S^{o}_{ads}/R + \ln 1/55.5)$. The calculated values of heat of adsorption and entropy of adsorption are listed in Table 4. Under the experimental conditions, the adsorption heat could be approximately regarded as the standard adsorption heat (ΔH^{o}_{ads}). The sign of enthalpy and entropy of adsorption both are positive. The positive values of ΔH^{o}_{ads} and ΔS^{o}_{ads} related to "substitutional adsorption" can be attributed to the increase in the solvent entropy and to a more positive water desorption enthalpy. Inspection of Table 4

revealed that increase in entropy is the driving force for the adsorption of all the three studied Schiff bases on the mild steel surface.

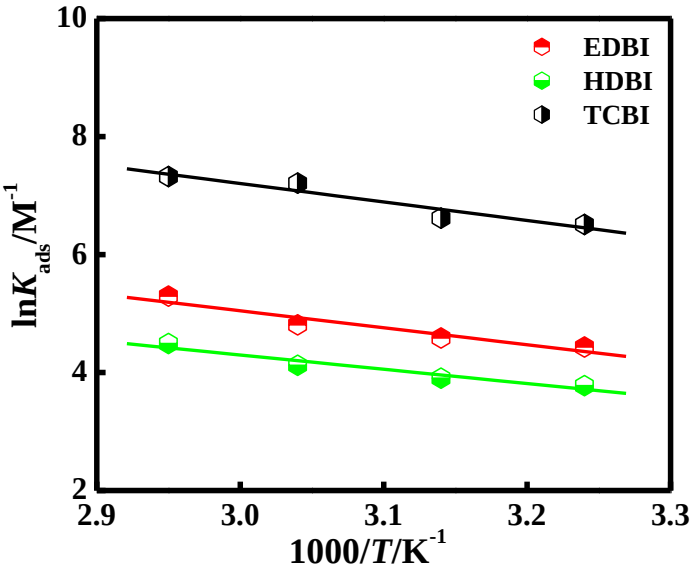

Figure 9. Adsorption isotherm plot for ln K_{ads} versus 1/T for adsorption of EDBI, HDBI and TCBI

3.5. Atomic force microscopy (AFM)

AFM is a powerful technique to investigate the surface morphology at nano to micro-scale and has become a new choice to study the influence of inhibitor on the generation and the progress of the corrosion at the metal/solution interface. Analysis of the images allowed quantification of surface roughness over area scales 12 × 12 μm^2. Atomic force microscope was used mainly for measuring three-dimensional topography. The three-dimensional AFM images are shown in Figure 10 a-e. As can be seen from Fig. 10 a-c, there was much less damage on the surface of mild steel with all the Schiff's bases as compared to mild steel surface dipped in 1 M HCl solution without inhibitor (Fig. 10d). The average roughness of polished mild steel surface (Fig. 10e) and, mild steel in 1 M HCl without inhibitor was calculated to be 66 and 395 nm respectively. However, in presence of 100 ppm concentration of all the three Schiff's base, the average roughness was reduced to 254, 285 and 195 nm respectively.

3.6 Scanning electron microscopy (SEM)

The SEM images of mild steel surfaces are given in Figure 11 a-e. As can be seen from Fig. 11 a-c (micrographs of mild steel surface in 1 M HCl solution with 100 ppm of inhibitors), there was much less damage on the surface of mild steel with all the Schiff's bases as compared to mild steel surface dipped in 1 M HCl solution without inhibitor (Fig. 11d). The Fig. 11 f showed polished mild steel surface.

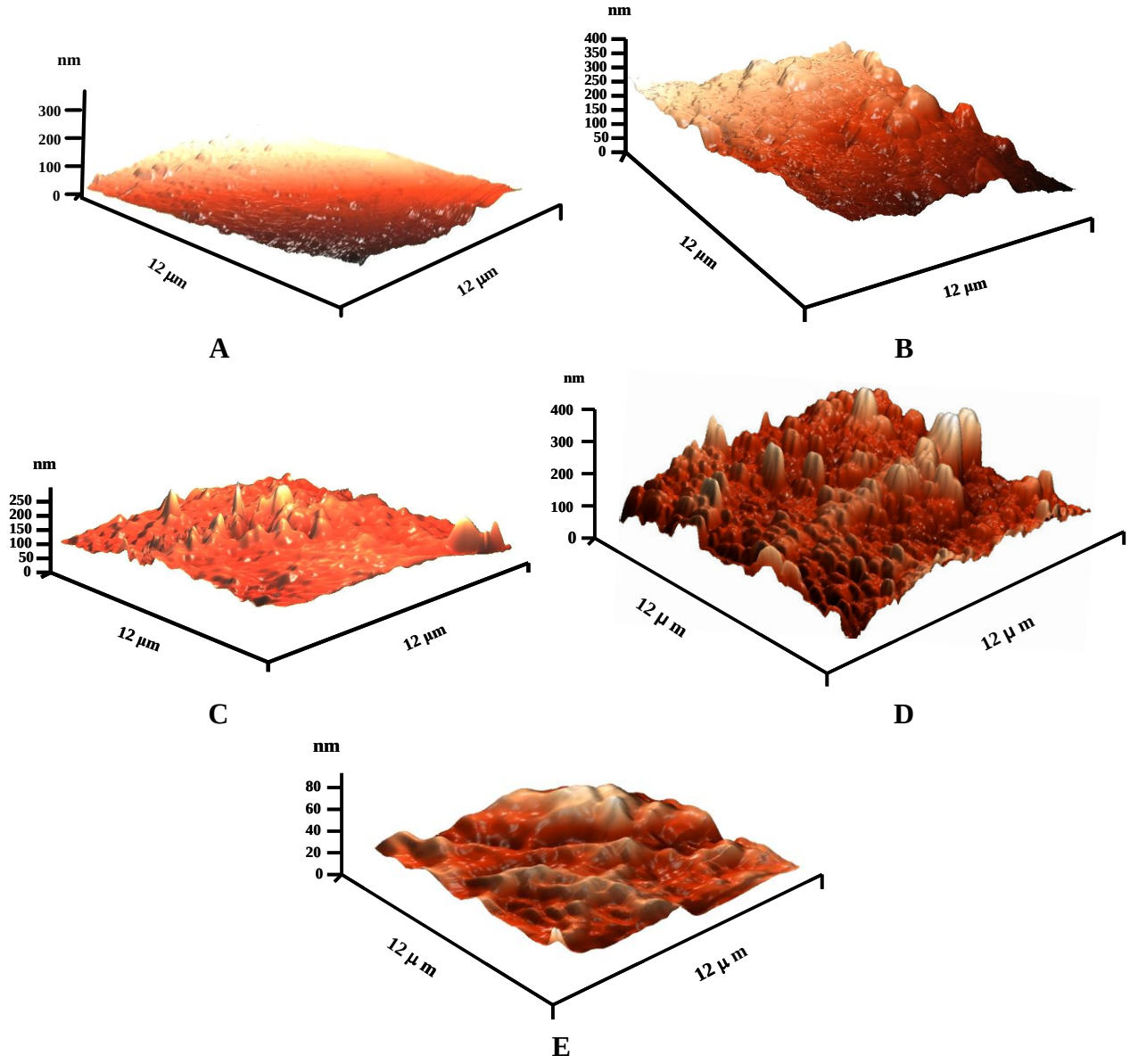

Figure 10. Atomic force micrographs of mild steel surface of (a) inhibited mild steel (1 M HCl + 100 ppm EDBI), (b) inhibited mild steel (1 M HCl + 100 ppm HDBI (c) inhibited mild steel (1 M HCl + 100 ppm TCBI), (d) mild steel in 1 M HCl and (e) polished mild steel

4. MECHANISM OF INHIBITION

Thermodynamic parameters showed that the adsorption of all the three studied Schiff's bases i.e. EDBI, HDBI and TCBI on the mild steel surface in 1 M HCl solution is chemical than physical one. Chemical adsorption of EDBI, HDBI and TCBI arises from the donor acceptor interactions between free electron pairs of hetero atoms and π-electrons of multiple bonds, vacant d-orbitals of S-atom (in case of TCBI) and vacant d-orbitals of Fe. In case of adsorption of organic compounds on the metallic surface, planarity of molecules must also be taken in to consideration. The difference in inhibition efficiency of EDBI and HDBI can be explained on the basis of molecular planarity.

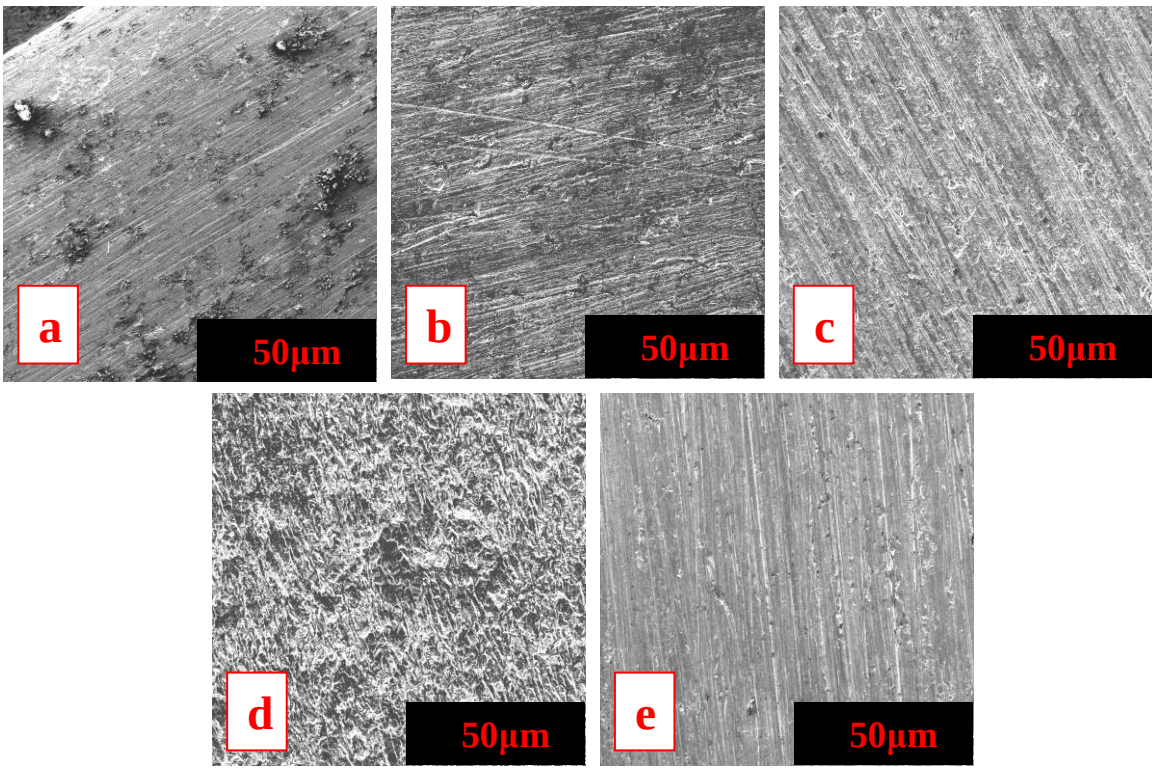

Figure 11. Scanning electron micrographs of mild steel surface of (a) inhibited mild steel (1 M HCl + 100 ppm EDBI), (b) inhibited mild steel (1 M HCl + 100 ppm HDBI (c) inhibited mild steel (1 M HCl + 100 ppm TCBI), (d) mild steel in 1 M HCl and (e) polished mild steel

The molecular structure of both EDBI and HDBI are almost identical except the carbon chain connecting indole nucleus. On account of molecular size, HDBI should show greater efficiency compared to EDBI, but it is not the case. EDBI molecule is almost planar (Figure 12) and hence adsorbed on the mild steel surface effectively. Whereas both aromatic nuclei are almost bending in HDBI molecule thus, HDBI molecule lost planarity and hence is not adsorbed as effectively as EDBI. An introduction of additional N-atoms as well as S-atom (vacant 3d-orbitals) offers more effective adsorption of TCBI molecule on the metallic surface. Thus the order of efficiency is TCBI > EDBI > HDBI.

The adsorption of organic molecules on the solid surfaces cannot be considered only as purely physical or as purely chemical adsorption phenomenon. In addition to the chemical adsorption, inhibitor molecules can also be adsorbed on the steel surface via electrostatic interaction between the charged metal surface and charged inhibitor molecule if it is possible. The free energy of adsorption value is around -40 kJ mol^{-1} hence, indicate contribution of physical adsorption. If the contribution of electrostatic interactions takes place, the following adsorption process can additionally be discussed.

Schiff bases have basic character and expected to be protonated in equilibrium with the corresponding neutral form in strong acid solutions.

$$SB+H^{+} \leftrightarrow SBH^{+} \quad (15)$$

Because mild steel surface carried positive charge, Cl^- ions should be first adsorbed onto the positively charged metal surface. Then the inhibitor molecules adsorb through electrostatic interactions between the negatively charged metal surface and positively charged Schiff base molecule. In this way, oxidation reaction can be prevented. The protonated Schiff base molecules are also adsorbed at cathodic sites of metal in competition with hydrogen ions. The adsorption of protonated Schiff base molecules reduces the rate of hydrogen evolution reaction. Finally, it should also be emphasized that, the large size and high molecular weight of Schiff base molecule can also contribute the greater inhibition efficiency of EDBI, HDBI and TCBI.

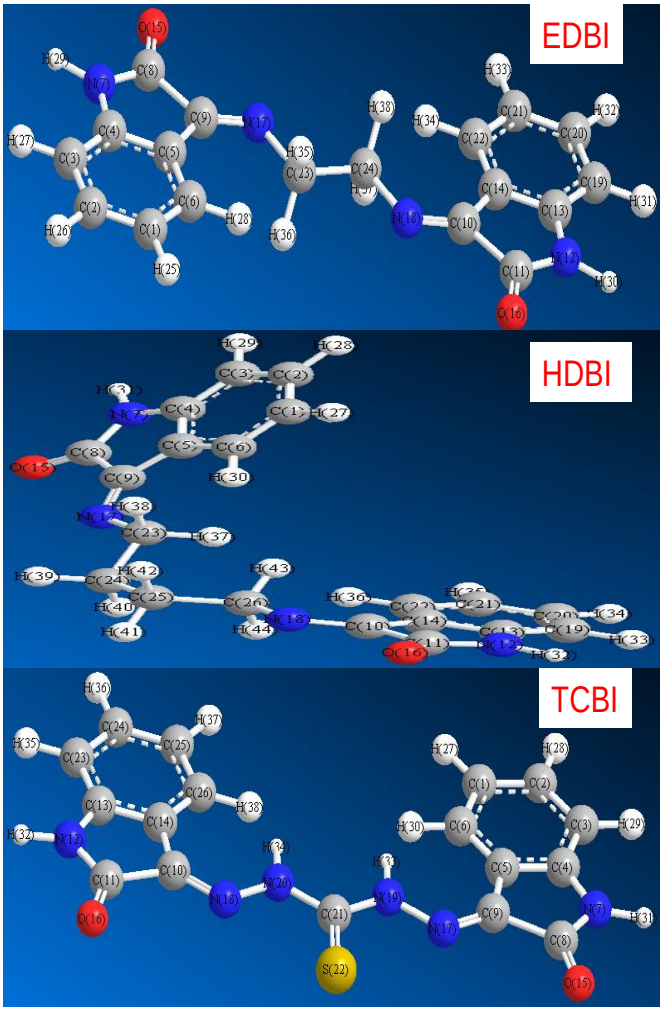

Figure 12. Three dimensional structure of EDBI, HDBI and TCBI

5. CONCLUSIONS

1. All the studied Schiff's bases have an excellent inhibition effect for the corrosion of mild steel in 1 M HCl. The high inhibition efficiencies of Schiff's bases were attributed to the adherent adsorption of the inhibitor molecules on the mild steel surface.

2. The adsorption of these compounds on the mild steel surface obeyed the Langmuir adsorption isotherm.
3. Potentiodynamic polarization studies revealed that all the three studied inhibitors are mixed type but predominantly cathodic inhibitors.
4. AFM and SEM micrographs of mild steel in 1 M HCl solution showed that addition of inhibitor to the aggressive solutions diminished the corrosion of mild steel.

References

1. M. Lagrene, B. Mernari, M. Bouanis, M. Traisnel, F. Bentiss, *Corros. Sci.* 44 (2002) 573
2. Z. Tao, S. Zhang, W. Li, B. Hou, Corros. Sci. 51 (2009) 2588.
3. A. Raman, P. Labine, Reviews on Corrosion Inhibitor Science and Technology, Vol. 1, NACE, Houston, TX, 1986, pp. 20.
4. M. Hosseini, S.F.L. Mertens, M. Ghorbani, M.R. Arshadi, *Mater. Chem. Phys*. 78 (2003) 800
5. A. K. Singh, M. A. Quraishi, *Corros. Sci*. 52 (2010) 152-160
6. A. K. Singh, M. A. Quraishi, E. E. Ebenso, *Int. J. Electrochem. Sci*. 6 (2011) 5673-5688
7. S. Ghareba, S. Omanovic, *Corros. Sci*. 52 (2010) 2104-2113,
8. F. Zucchi, G. Trabanelli, G. Brunoro, *Corros. Sci*. 33 (1992) 1135-1139
9. J. Aljourani, M.A. Golozar, K. Raeissi, *Mater. Chem. & Phys*. 121 (2010) 320 -325
10. M.N.H. Moussa, A.A. El-Far, A.A. El-Shafei, *Mater. Chem. & Phys*. 105 (2007) 105-113.
11. A. K. Singh, S. K. Shukla, M. A. Quraishi, E. E. Ebenso, *J. Taiwan Inst. Chem. Eng*. (2011), doi:10.1016/ j.jtice.2011.10.012
12. E. Naderi, M. Ehteshamzadeh, A.H. Jafari, M.G. Hosseini, *Mater. Chem. Phys*. 120 (2010) 134
13. K.S. Jacob, G. Parameswaran, *Corros. Sci*. 52 (2010) 224
14. M. Behpour, S.M. Ghoreishi, N. Mohammadi, N. Soltani, M. Salavati-Niasari, *Corros. Sci*. 52 (2010) 4046-4057
15. V. P. Singh, P. Singh, A. K. Singh, *Inorg. Chim. Acta* (2011), doi:10.1016/j.ica.2011.09.037
16. A. K. Singh, M. A. Quraishi, *Corros. Sci*. 52 (2010) 1529-1535
17. C. Deslouis, B. Tribollet, G. Mengoli, M. M. Musiani, *J. Appl. Electrochem*. 18 (1988) 374-383
18. S. S. Abdel Rehim, H. H. Hassan, M. A. Amin, *Appl. Surf. Sci*., 187 (2002) 279-290
19. A. K. Singh, M. A. Quraishi, *Corros. Sci*. 52 (2010) 1373-1385.
20. H. Ashassi-Sorkhabi, D. Seifzadeh, M. G. Hosseini, *Corros. Sci*. 50 (2008) 3363-3370
21. A. K. Singh, M. A. Quraishi, *J. Appl. Electrochem*. 40 (2010) 1293-1306
22. A. K. Singh, M. A. Quraishi, *Mater. Chem. Phys*. 123 (2010) 666-677
23. E. S. Ferreira, C. Giancomelli, F. C. Giacomelli, A. Spinelli, *Mater. Chem. Phys*. 83 (2004) 129-134
24. W. H. Li, Q. He, C. L. Pei, B. R. Hou, *J. Appl. Electrochem.* 38 (2008) 289-295
25. A. K. Singh, M. A. Quraishi, *J. Appl. Electrochem*. 41 (2011) 7-18
26. A. K. Singh, M. A. Quraishi, *Corros. Sci*. 53 (2011) 1288-1297.
27. N.P. Clark, E. Jakson, M. Robinson, *Br. Corros. J*. 14 (1979) 33.
28. T. Szauer, A. Brandt, *Electrochim. Acta* 26 (1981) 253
29. M. Abdallah, *Corros. Sci*. 44 (2002) 717
30. G. Avci, *Mater. Chem. Phys*. 112 (2008) 234–238
31. A. Yurt, A. Balaban, S. Ustün Kandemir, G. Bereket, B. Erk, *Mater. Chem. Phys*. 85 (2004) 420–426
32. L. Tang, G. Mu, and G. Liu, *Corros. Sci*. 45 (2003) 2252